THE JOURNAL OF PHYSICAL CHEMISTRY A

Article

pubs.acs.org/JPCA

On the Size and Structure of Helium Snowballs Formed around Charged Atoms and Clusters of Noble Gases

Peter Bartl,[†,§] Christian Leidlmair,[†,#,§] Stephan Denifl,[†,§] Paul Scheier,*[,†] and Olof Echt*[,†,‡]

[†]Institut für Ionenphysik und Angewandte Physik, University of Innsbruck, Technikerstrasse 25, A-6020 Innsbruck, Austria

[‡]Department of Physics, University of New Hampshire, Durham, New Hampshire 03824, United States

ABSTRACT: Helium nanodroplets doped with argon, krypton, or xenon are ionized by electrons and analyzed in a mass spectrometer. $He_nNg_x^+$ ions containing up to seven noble gas (Ng) atoms and dozens of helium atoms are identified; the high resolution of the mass spectrometer combined with advanced data analysis make it possible to unscramble contributions from isotopologues that have the same nominal mass but different numbers of helium or Ng atoms, such as the magic $He_{20}{}^{84}Kr_2^+$ and the isobaric, nonmagic $He_{41}{}^{84}Kr^+$. Anomalies in these ion abundances reveal particularly stable ions; several intriguing patterns emerge. Perhaps most astounding are the results for He_nAr^+, which show evidence for three distinct, solid-like solvation shells containing 12, 20, and 12 helium atoms. This observation runs counter to the common notion that only the first solvation shell is solid-like but agrees with calculations by Galli et al. for He_nNa^+ [*J. Phys. Chem. A* **2011**, *115*, 7300] that reveal three shells of icosahedral symmetry. $He_nAr_x^+$ ($2 \le x \le 7$) ions appear to be especially stable if they contain a total of $n + x = 19$ atoms. A sequence of anomalies in the abundance distribution of $He_nKr_x^+$ suggests that rings of six helium atoms are inserted into the solvation shell each time a krypton atom is added to the ionic core, from Kr^+ to Kr_3^+. Previously reported strong anomalies at $He_{12}Kr_2^+$ and $He_{12}Kr_3^+$ [Kim, J. H.; et al. *J. Chem. Phys.* **2006**, *124*, 214301] are attributed to a contamination. Only minor local anomalies appear in the distributions of $He_nXe_x^+$ ($x \le 3$). The distributions of He_nKr^+ and He_nXe^+ show strikingly similar, broad features that are absent from the distribution of He_nAr^+; differences are tentatively ascribed to the very different fragmentation dynamics of these ions.

1. INTRODUCTION

The mobility of positively charged ions X^+ injected into liquid ^{4}He differs markedly from that of ions in liquid ^{3}He. The temperature and field dependence of the mobility suggests that a cation in ^{4}He will drag with it some 50 He atoms, which, as a result of electrostriction, form a solid-like layer.[1] In subsequent work, it was found that the size of this "snowball" depends on the electronic structure of the core ion.[2]

An alternate and in some way more accurate approach to determine the number of atoms in a snowball is via gas-phase experiments; they can provide information about dissociation (or evaporation or separation) energies defined as

$$D_n = E_{n-1} - E_n \quad (1)$$

where E_n is the total energy of He_nX^+. Dissociation energies (or, more exactly, enthalpies) may be derived quantitatively from van't Hoff plots by measuring the partial pressure of He_nX^+ in thermal equilibrium as a function of temperature.[3] Unfortunately, these measurements are limited to very small complexes.

A simpler method to determine the number of helium atoms in a partial or complete solvation shell is to look for anomalies in the abundance distribution of He_nX^+ measured under nonequilibrium conditions; abundance anomalies often correlate with anomalies in D_n. For example, Kojima et al. injected Ar^+ or Kr^+ into a drift tube filled with helium gas at low density (about 2 Pa) and low temperature (4.4 K); the noble gas (Ng) ions were found to bind up to 14 helium atoms.[4] The abundance distributions depended on experimental conditions (helium pressure, temperature, applied electric field), but for suitable choice of the drift field, abrupt drops in the abundance were observed at $He_{12}Ar^+$ and $He_{12}Kr^+$. The same ions were also formed prominently when helium droplets were doped with Ar or Kr and ionized by electrons.[5−8] The agreement between these two different experimental approaches stems from the fact that in both cases, the observed ions are dissociation products of larger precursor ions. Dissociation in the drift tube is induced by collisions of the ions with the buffer gas, whereas in mass spectra of doped helium droplets, dissociation is the result of the excess energy introduced upon ionization. The relation between the size dependence of dissociation energies D_n and ion abundances I_n in experiments where cluster ions undergo unimolecular dissociation has been explored by several authors.[9−14] For complexes with very low heat capacities, local anomalies in I_n directly correlate with local anomalies in D_n.[15,16]

Experiments involving doped helium droplets have revealed anomalies in the abundance of He_nX^+ for many ions X^+,

Special Issue: A. W. Castleman, Jr. Festschrift

Received: July 2, 2013
Revised: September 4, 2013
Published: October 15, 2013

   dx.doi.org/10.1021/jp406540p | *J. Phys. Chem. A* 2014, 118, 8050−8059

including alkali ions and their dimers,[16−19] other metal ions,[20] halogen ions,[21] H^+, H_2^+, and H_3^+,[22] other polyatomic ions,[21] and C_{60}^+, C_{70}^+, and their aggregates.[15,23] Here, n = 12 is a frequently observed anomaly, often interpreted to indicate formation of a solvation shell with icosahedral symmetry,[22,24] but the number of helium atoms in the first solvation shell may be much larger. For example, 18−20 atoms are needed to complete the first solvation shell for Mg^+,[20,25] 20 for I_2^+,[21] 60 for C_{60}^+, and 62 for C_{70}^+.[15,26,27] On the other hand, much smaller anomalies may indicate closure of subshells or formation of stable structures such as, at n = 2, the formation of the linear $[He−Na−Na−He]^+$, followed by an anomaly at n = 6 when a subshell is completed.[16,28]

The richness of anomalies observed for some metallic ions[16,20] contrasts with the small set of anomalies reported so far for Ng's. Here, n = 12 is the only anomaly observed for He_nAr^+ and He_nKr^+ (pronounced anomalies were reported[7] for $He_{12}Kr_2^+$ and $He_{12}Kr_3^+$, but we will show that they were caused by xenon impurities). No anomaly was found for He_nNe^+ if doped helium droplets were ionized[29−31] even though drift tube experiments indicated enhanced stability of $He_{13}Ne^+$.[4] In a separate publication,[32] we have solved this discrepancy; it arises from the difficulty to resolve nominally isobaric ions. In fact, the paucity of anomalies reported for He_nNg^+ can be traced to the challenge of deducing ion abundances from mass spectra; (i) for all Ng's, the mass number of the most abundant isotope (^{20}Ne, ^{40}Ar, ^{84}Kr, and ^{132}Xe) is an integer multiple of the ^{4}He mass number, and (ii) the large number of naturally occurring isotopes of Kr (6) and Xe (9) causes a multitude of mass spectral coincidences for heavy Ng's. Several ions, differing in the number of helium atoms and/or the number of Ng atoms, will have the same nominal mass.

The resolving power of the mass spectrometer employed in the present work exceeds that of instruments used previously by an order of magnitude. As a result, ions containing different numbers of Ng atoms can be resolved; a large number of anomalies are identified in the abundance distributions of $He_nNg_x^+$. Some intriguing patterns emerge from these data. Perhaps the most surprising ones are anomalies in the He_nAr^+ series at n = 32 and 44, in addition to the well-known anomaly of $He_{12}Ar^+$. It is tempting to assign the anomalies to three solvation shells of (approximately) icosahedral symmetry, with 20 atoms localized in the hollow sites of the $He_{12}Ar^+$ icosahedron, thus forming a dodecahedron, and an additional 12 atoms localized in the hollow sites of $He_{32}Ar^+$, thus forming an icosahedron; the two outer shells thus resemble the commensurate phase of helium on C_{60}^+, which offers 20 hexagonal and 12 pentagonal adsorption sites.[15,26,27] The interpretation draws on a recent path integral Monte Carlo study by Galli et al.[25] who concluded that three distinct solvation shells of icosahedral symmetry arrange around Na^+, but no other alkali and alkali-earth ions were found to exhibit such a high degree of order. In fact, early experimental work suggested that no more than two shells are part of the snowball,[2] and many recent theoretical studies of ions solvated in helium concluded that no structural order exists outside of the first solvation shell.[33,34] Even in the first layer, quantum effects may destroy structural order and wash out shell effects.[31,35−37] We note that these theoretical studies included quantum effects (zero-point motion and the bosonic nature of helium) to various degrees, which explains some of the differences between them.

Several other anomalies in distributions of $He_nNg_x^+$ are reported and interpreted in this work. The solvation layer of $He_nKr_x^+$ appears to grow by insertion of six-membered helium rings as the ionic core grows from x = 1 to 2 to 3, and helium−argon complexes containing at least 2 Ar atoms appear to be particularly stable if they contain a total of 19 atoms. Striking differences are found between the abundance distributions of He_nNg^+ for the heavy Ng's (Kr, Xe) and He_nAr^+; a parallel to the different fragmentation dynamics of these systems is tentatively drawn.[38,39] We also critically evaluate previously published mass spectra and include recent results for $He_nNe_x^+$.[32] So far, few quantum mechanical treatments of $He_nNg_x^+$ have been reported; the nature of the ionic core, charge delocalization, vibrational delocalization, and other quantum mechanical effects pose significant challenges. It is to be hoped that results presented in this work will provide critical tests for future theoretical work.

2. EXPERIMENT

Neutral helium nanodroplets were produced by expanding helium (purity 99.9999%) from a stagnation pressure of about 2 MPa through a 5 μm nozzle, cooled by a closed-cycle refrigerator (Sumitomo Heavy Industries LTD, model RDK-415D) to about 10 K, into vacuum. The average number of atoms per droplet formed in the expansion ranged from a few × 10^4 to 10^6;[40] these droplets are superfluid with a temperature of ∼0.37 K.[40] The resulting supersonic beam was skimmed by a 0.8 mm conical skimmer, located 12 mm downstream from the nozzle. The skimmed beam traversed a 20-cm-long pick-up region into which either argon (Air Liquide, purity 99.9999%), krypton (99.999%), or xenon (99.999%) was introduced at a partial pressure of a few tenths of a millipascal. After the pick-up region, the doped helium droplets passed a region in which they were ionized by collisions with electrons at energies ranging from 70 to 140 eV. Further details will be specified in the figure captions.

Cations were accelerated to 40 eV into the extraction region of a commercial time-of-flight mass spectrometer equipped with a reflectron (Tofwerk AG, model HTOF); its mass resolution was $\Delta m/m$ = 1/7000. The base pressure in the mass spectrometer was 10^{-5} Pa. The ions were extracted at 90° into the field-free region of the spectrometer by a pulsed extraction voltage. At the end of the field-free region, they entered a two-stage reflectron that reflected them toward a microchannel plate detector operated in single-ion counting mode. Additional experimental details have been described elsewhere.[41,42]

3. RESULTS AND DISCUSSION

A. Mass Spectra and Data Analysis. In the past, most attempts to identify Ng−helium complexes $He_nNg_x^+$ of enhanced stability have been hampered by the inability to resolve different ions with the same nominal mass. Helium is essentially monisotopic (the natural abundance of ^{4}He is 99.999863%). Argon is the only other Ng that is nearly monisotopic, with ^{40}Ar at 99.600% and ^{36}Ar at 0.337%. Even so, the nominal mass of $He_{12}Ar^+$, which appears prominently in mass spectra, coincides with that of He_{22}^+ and $He_2Ar_2^+$. The exact masses differ by 0.064 au; a resolution of 1/1400 or better would be needed to separate the ions.

The problem is aggravated in experiments with krypton and xenon, which have 6 and 9 naturally occurring isotopes, respectively. To make things worse, the masses of their most

dx.doi.org/10.1021/jp406540p | J. Phys. Chem. A 2014, 118, 8050−8059

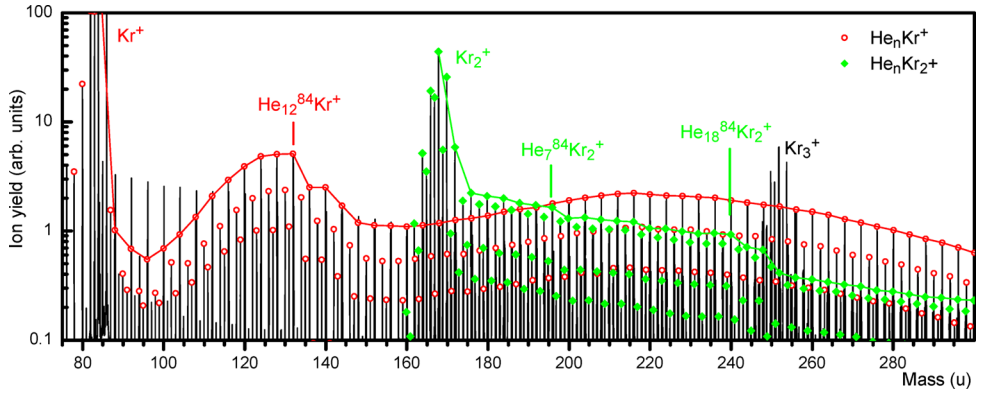

Figure 1. A mass spectrum of helium nanodroplets doped with krypton. Isotopologues due to He_nKr^+ and $He_nKr_2^+$ ($n \geq 0$) are marked by open circles and solid diamonds, respectively; mass peaks due to the most abundant isotopologues in each series, containing one or two ^{84}Kr, are connected by lines. Some anomalies in the ion yield are marked. Experimental conditions: helium pressure 1.6 MPa, nozzle temperature 8.9 K, krypton pressure 0.2 mPa (corrected ion gauge value).

abundant isotopes, ^{84}Kr and ^{132}Xe (relative abundance of 57 and 26.89%, respectively) are integer multiples of the helium mass. In past research,[7,43,44] the ions could not be separated from He_{21} and He_{33}, which are heavier by just 0.143 and 0.182 au, respectively. In the present experiments, an instrument with resolution $\Delta m/m \approx 1/7000$ is used, and these ions are easily resolved. This is demonstrated in Figure 1, which displays a mass spectrum of helium nanodroplets doped with krypton. The isotopes of Kr are ^{78}Kr (0.3%), ^{80}Kr (2.3%), ^{82}Kr (11.6%), ^{83}Kr (11.5%), ^{84}Kr (57.0%), and ^{86}Kr (17.3%). The ion series He_n^+, He_nKr^+, $He_nKr_2^+$, and $He_nKr_3^+$ are observed. The He_n^+ series forms the dominant peaks below 80 au and between 88 and 108 au. Peaks due to isotopologues of He_nKr^+ ($n \geq 0$) are marked by open dots; those due to the main isotope, $He_n{}^{84}Kr^+$, are connected by lines.[45] An abrupt drop in the ion yield between $He_{12}{}^{84}Kr^+$ and $He_{13}{}^{84}Kr^+$ is clearly visible; a weaker drop occurs at $n = 14$.

Peaks due to isotopologues of $He_nKr_2^+$ are marked by full diamonds; those due to the main isotopologue, $He_n{}^{84}Kr_2^+$, are connected by lines.[45] Anomalies at $n = 7$ and 18 are marked. An even stronger anomaly occurs at $n = 20$. The corresponding ion peaks coincide with isotopologues of Kr_3^+ in nominal mass, but they are resolved.

A close-up of the mass spectrum is shown in Figure 2a. Isotopes due to He_nKr^+ are marked by open dots; they are fully resolved from isotopologues of $He_nKr_2^+$, which are marked by diamonds and connected by a line.[45] Peaks due to pure He_n^+ (not marked) appear immediately to the right of $He_n{}^{84}Kr^+$ (mass difference 0.143 au).

A problem in measurements of krypton- or xenon-doped helium droplets is crosstalk between ions containing the same number x of Ng atoms but different numbers of helium atoms. This is illustrated in Figure 2b, which shows a simulated spectrum of $He_nKr_2^+$ (narrow bars connected by solid lines). The ion yield of the dominant isotopologue, $He_n{}^{84}Kr_2$, was set to 1 for all values of n. The contributions of $He_{12}Kr_2^+$ are represented by the wide bars in Figure 2b. Its isotopologues cover a wide mass range; three of them contribute to the signal at 212 au, namely, $He_{12}{}^{82}Kr_2^+$, $He_{12}{}^{80}Kr^{84}Kr^+$, and $He_{12}{}^{78}Kr^{86}Kr^+$. Their masses differ by less than 0.01 au from that of $He_{11}{}^{84}Kr_2^+$, which provides the dominant contribution at 212 au; these ions cannot be resolved. Other isotopologues that also contribute at 212 au are $He_{11}{}^{82}Kr^{86}Kr^+$ and $He_{10}{}^{86}Kr_2^+$.

We disentangle the various contributions from these ions by applying a matrix method.[42,46,47] In essence, the ion yield measured by a mass spectrum represents the ion abundance of $He_nKr_x^+$ convoluted with the isotopologues of Kr_x; therefore, the ion abundance can be extracted from a mass spectrum by a deconvolution.

B. Abundance of Ng^+ and Ng_x^+ Complexed with Helium. Figures 3−5 display the ion abundances of $He_nAr_x^+$ ($x \leq 7$), $He_nKr_x^+$ ($x \leq 3$), and $He_nXe_x^+$ ($x \leq 3$). As described in section 3A, the data are corrected for crosstalk from isotopologues. Reproducible anomalies are marked and listed in Table 1 together with previously reported anomalies, including recent data for $He_nNe_x^+$.[32] As discussed in section 3D, abrupt changes in the abundance are expected to correlate with abrupt changes in the dissociation (or separation or evaporation) energies as defined in eq 1. These abrupt changes often correlate with closure of solvation shells or subshells.

For each Ng, we have recorded several mass spectra, varying the initial size of the helium droplets by varying the stagnation pressure and/or temperature and the partial pressure of the Ng in the pick-up region. These conditions did not significantly affect the anomalies in the ion abundance, although it should be mentioned that droplet sizes remained within the somewhat narrow range of 10^5−10^6. Another parameter that could potentially play a role is the time that elapses between formation of the ions in the ionizer and the mass analysis, that is, the time at which they are extracted into the time-of-flight mass spectrometer. In the present work, this time amounts to about 10^{-4} s; it could not be varied.

B.1. Argon. For helium−argon complexes, the only magic number firmly established so far was $He_{12}Ar^+$. The anomaly was observed when mass-selected atomic ions were injected into helium gas at 4.4 K,[4] and in mass spectra of helium droplets doped with argon.[5,6,48] It is clearly reproduced in our data (Figure 3). According to calculations by Murrell et al.,[49] $He_{12}Ar^+$ has enhanced stability. The authors applied the diatomics-in-molecules method in order to determine the classical ground-state structures of He_nAr^+ up to $n = 16$. The ionic core in He_nAr^+ is the trimeric, symmetric ($D_{\infty h}$ symmetry) $[He{-}Ar{-}He]^+$, although charge delocalization in this complex is very small, much smaller than that in $[He{-}Ne{-}He]^+$. For $HeAr^+$, Sun et al.[50] calculated that 99.6% of the charge resides on the argon.

dx.doi.org/10.1021/jp406540p | J. Phys. Chem. A 2014, 118, 8050−8059

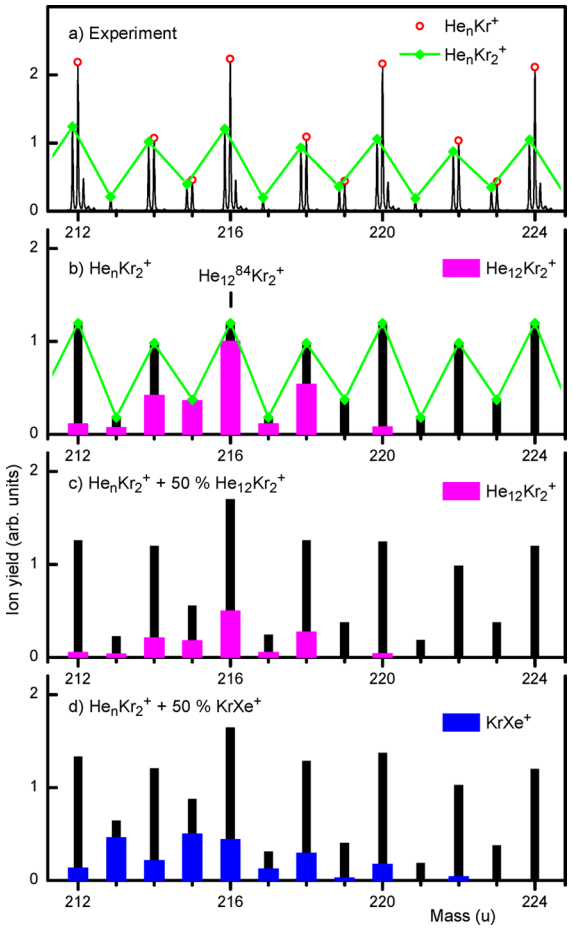

Figure 2. (a) A section of a mass spectrum of helium nanodroplets doped with krypton. Isotopologues due to He_nKr^+ and $He_nKr_2^+$ are marked by open circles and solid diamonds, respectively; mass peaks due to $He_nKr_2^+$ isotopologues are connected by lines. (b–d) Narrow bars: Simulated mass spectra of $He_nKr_2^+$ assuming unit mass resolution. Panel b assumes equal contributions for all sizes n; the wide bars represent the contribution of $He_{12}Kr_2^+$ to the total spectrum. Mass peaks are connected by lines in order to demonstrate the similarity with the experimental pattern observed for $He_nKr_2^+$ in panel a (solid diamonds). Panel c assumes that the abundance of $He_{12}Kr_2^+$ is enhanced by 50% relative to other sizes; this extra contribution is represented by wide bars. Panel d assumes that a 50% $KrXe^+$ contamination is present; this extra contribution is represented by wide bars.

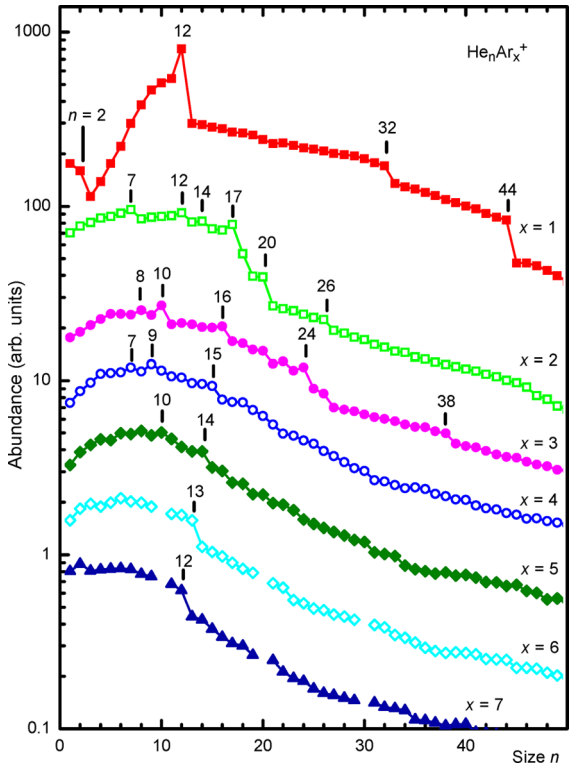

Figure 3. Ion abundance of $He_nAr_x^+$ with $1 \leq x \leq 7$; reproducible anomalies are marked. Experimental conditions were helium pressure 2 MPa (1.6 MPa), nozzle temperature 10 K (9.1 K), Ar pressure (corrected ion gauge reading) 0.56 mPa (0.21 mPa), and electron energy 70 eV (100 eV); values in parentheses pertain to He_nAr^+.

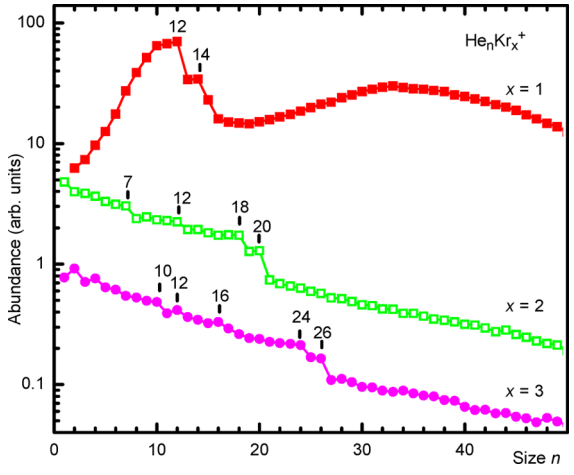

Figure 4. Ion abundance of $He_nKr_x^+$ ($1 \leq x \leq 3$) extracted from mass spectra and corrected for the occurrence of isotopologues. Reproducible anomalies are marked. Experimental conditions were helium pressure 1.6 MPa, nozzle temperature 8.9 K (9 K), Kr pressure (corrected ion gauge reading) 0.20 mPa, and electron energy 70 eV.

In $He_{12}Ar^+$, the trimeric core is surrounded by two rings of five helium atoms each.[49] The calculated dissociation energies of He_nAr^+ (which do not include the effects of zero-point motion) are displayed in Figure 6a. Completion of the ionic core at n = 2 and completion of the first solvation shell at n = 12 are accompanied by abrupt drops in D_n, in agreement with abrupt drops in the ion abundance (Figure 3). According to Murrell et al., two more helium atoms can be squeezed into the first shell before helium–helium repulsion pushes additional atoms into a second shell.[49] The drop in the calculated dissociation energies at n = 14 is not reflected in the experimental data.

Instead, the experiment reveals strong anomalies at n = 32 and 44; they are outside of the size range of previous experimental and theoretical investigations. We propose an appealing structural model for these magic numbers, inspired by a path integral Monte Carlo study of He_nNa^+ by Galli et al.[25]

When applied to quantum systems of bosons, the method can provide exact estimates for properties, within the statistical uncertainties of the Monte Carlo calculation and the accuracy of the assumed interaction potential. According to the calculations by Murrell et al.,[49] the distance between Ar^+ and the two He atoms in the trimeric core is not much less than that between Ar^+ and the other, neutral He atoms in $He_{12}Ar^+$. Thus, $He_{12}Ar^+$ has approximately icosahedral symmetry. An

dx.doi.org/10.1021/jp406540p | J. Phys. Chem. A 2014, 118, 8050–8059

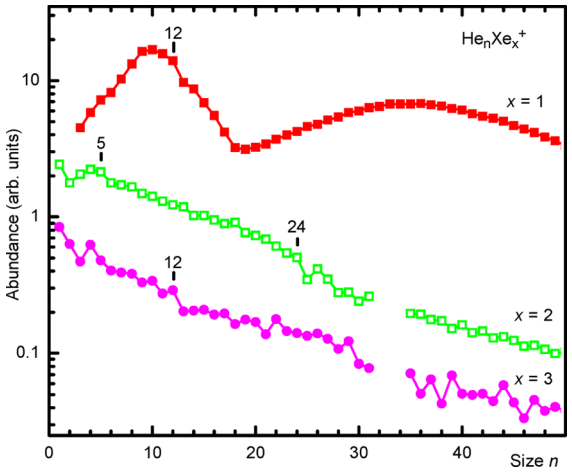

Figure 5. Ion abundance of $He_nXe_x^+$ ($1 \le x \le 3$) extracted from mass spectra and corrected for the occurrence of isotopologues. Reproducible anomalies are marked. Experimental conditions were helium pressure 1.6 MPa, nozzle temperature 8.9 K, Xe pressure (corrected ion gauge reading) 0.17 mPa (0.24 mPa), and electron energy 70 eV; values in parentheses pertain to $He_nXe_3^+$.

icosahedron has 12 vertices and 20 triangular faces. If these faces are decorated by one He atom each, one obtains a dodecahedral $He_{32}Ar^+$ (20 vertices, 12 pentagonal faces). If the faces of this complex are decorated by one He atom each, one obtains the magic $He_{44}Ar^+$, with a total of three closed solvation shells. This description ignores the quantum nature of helium, but it agrees with the findings for He_nNa^+ by Galli et al.,[25] namely, the existence of three distinct shells, angular order of helium within each shell, and structural correlation between the shells. Each layer provides a corrugated surface for the next layer, which remains essentially rigid; exchange of atoms within a shell and between shells is small. This type of growth of concentric shells of icosahedral symmetry is not energetically favored for neutral clusters that interact via a Lennard-Jones or similar potentials[51] but is driven by the strong interaction of helium with the charge at the center.[25] It is also interesting to note that a commensurate layer of 32 helium atoms adsorbed on C_{60}^+ (which plays the role of $He_{12}Ar^+$) features the same arrangement, namely, 20 atoms located at the centers of the carbon hexagons plus 12 atoms located at the centers of the carbon pentagons.[15,26,27] The rigidity of the helium layer is caused by the strong corrugation of the C_{60}^+ surface. In this

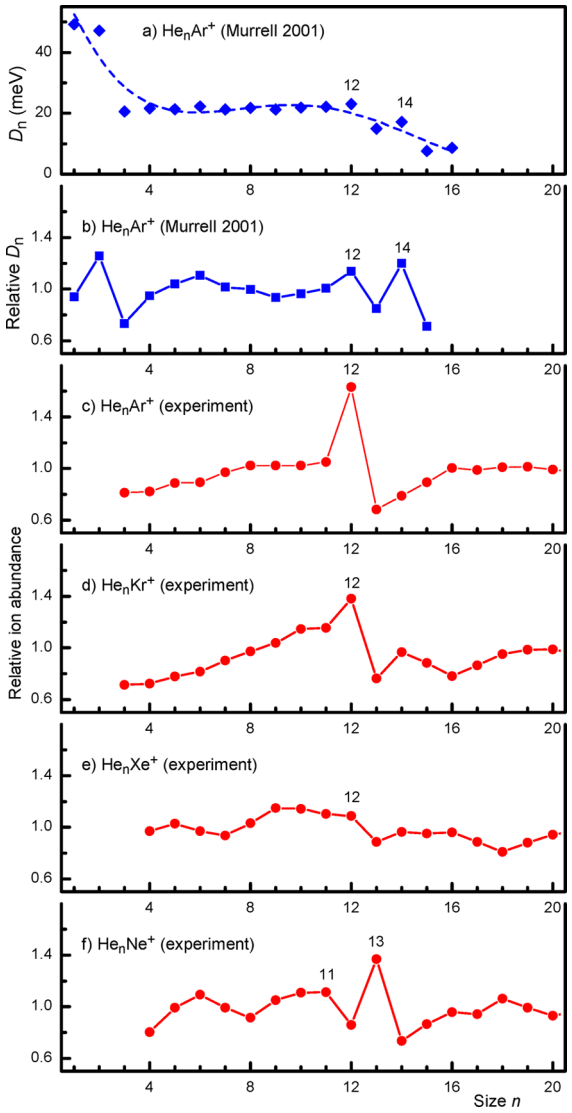

Figure 6. Summary of experimental results and comparison with theory. (a) Dissociation energies D_n calculated for He_nAr^+;[49] the dashed line represents the local average of D_n. (b) Relative dissociation energies of He_nAr^+, that is, the calculated values[49] divided by the local average. (c–f) Relative experimental ion abundances of He_nNg^+ for Ar, Kr, Xe, and Ne (from ref 32).

Table 1. Sizes n at Which the Ion Abundance of $He_nNg_x^+$ versus n Exhibits Local Maxima or Abrupt Drops[a]

x	Ne[m]	Ar	Kr	Xe
1	**11**, **13**	**2**, **12**, 32, **44**	**12**, **14**	12
lit	exp: 11[b], 13[b], none[c,d] theory: 7[e], 10[e], 12[e], none[d,f]	exp: 12[b,g,h] theory: 2[e], 12[e], 14[e]	exp: 10[k], 12[b,j,i]	exp: 4[k], 8[k], 15[k], none[j,l]
2	**12**, **14**	7, 12, 14, **17**, **20**, 26	**7**, 12, **18**, **20**	**24**
lit	exp: none for $n \le 5$[c]		exp: 12[j]	exp: none[j]
3	**5**, **11**	8, **10**, **16**, 24, 26	10, 12, 16, **24**, **26**	12
lit			exp: 12[j]	
4	8	7, 9, **15**		
5	8, **14**	10, **14**		
6	7	**13**		
7	**6**, 12	**12**		

[a]Bold font indicates strong anomalies. Previously published values are listed in rows preceded by lit. Data for neon are from ref 32. [b]Reference 4. [c]Reference 29. [d]Reference 31. [e]Reference 49. [f]Reference 30. [g]Reference 5. [h]Reference 6. [i]Reference 6. [j]Reference 7. [k]Reference 43. [l]44. [m]Reference 32.

dx.doi.org/10.1021/jp406540p | J. Phys. Chem. A 2014, 118, 8050–8059

case, though, the two shells (containing 20 and 12 atoms, respectively) have nearly the same dissociation energies and radial distances from the center; they appear as just one shell in the experiment.[15] We also mention a study of C_{28}, which has 12 pentagonal plus 4 hexagonal hollow sites. It features 16 energetically preferred sites, but another anomaly in the computed dissociation energy occurs when 32 helium atoms form a single, ordered layer of icosahedral symmetry.[52]

The fact that anomalies as large as $n = 44$ are observed is remarkable because they suggest an unusually large rigid core surrounding the ion. Most theoretical studies of cations solvated in helium concluded that the solid-like structure does not extend beyond the first shell; atoms in the second shell are more delocalized and liquid-like. Gianturco and co-workers[33,34] employed the variational Monte Carlo method and ab initio potential energy curves to optimize a trial wave function; in a second step, they applied the diffusion Monte Carlo algorithm in order to obtain the energy and the geometric distributions of the cluster. They found a rigid solvation shell of icosahedral symmetry for $He_{12}Na^+$, but delocalization in the first shell increases if the number of helium atoms is smaller or larger than 12.[34] However, the microscopic structure of the snowball is strongly dependent on the identity of the ion; shells around Na^+ were found to be the most distinct, as judged from the radial density distributions and angular correlations.[25] Further theoretical work will be needed to confirm that the structure of the snowball around Ar^+ is, indeed, similar to the one predicted[25] for Na^+.

Two further remarks are in order. First, anomalies at $n = 12$, 32, and 44 were already reported for He_nAg^+, plus another one at $n = 10$.[20] A very different model, including electronic excitations of the ion, had been invoked in the interpretation; no attempt was made to assign a structure. Second, the ion abundance of He_nNa^+ has been reported by our group for $n \leq 27$; it displays distinct anomalies at $n = 2$ and 12.[16] We have inspected the mass spectra once again, but no reliable information can be drawn for complexes with $n > 27$.

Several anomalies are observed in Figure 3 for $He_nAr_2^+$, with the strongest ones at $n = 17$ and 20. Several experimental and theoretical studies of argon cluster ions have been reported (see, e.g., ref 53 for recent work), but we are not aware of any experimental or theoretical work pertaining to $He_nAr_x^+$ with $x \geq 2$ except for a theoretical study of the linear $[Ar{-}He{-}Ar]^+$ ion by Sun et al.[50] This ion is bound by only $E = -0.063$ eV,[50] a factor of 20 less than the energy of Ar_2^+.[54,55] Thus, $[Ar{-}He{-}Ar]^+$ would be metastable; the most likely ionic core in $He_nAr_2^+$ is the argon dimer ion. We refrain from speculating about the structure of "magic" $He_nAr_x^+$ ($x \geq 2$). However, one interesting feature is apparent from Figure 3, namely, the gradual decrease of the magic number $n = 17$ for $x = 2$ to $n = 16$ for $x = 3$, $n = 15$ for $x = 4$, and so on to $n = 12$ for $x = 7$. In other words, the complex with a total of $n + x = 19$ atoms has enhanced stability. In fact, the smallest magic number consistently identified in experiments involving pure argon is Ar_{19}^+; it is usually assumed to have the structure of a double icosahedron.[56−60] It is conceivable that the linear structure of Ar_3^+ and Ar_4^+[60−63] stabilizes the double icosahedron for helium−argon complexes containing up to $x = 4$ argon atoms and $19 - x$ helium atoms, but it is not at all clear why the replacement of further helium atoms with argon atoms should preserve the structure and high stability of the double icosahedron, given the very different polarizabilities of He and Ar.

B2. Krypton. When krypton ions are injected into low-pressure helium gas at 4.4 K, He_nKr^+ containing up to 14 helium atoms form. The abundance of $He_{12}Kr^+$ greatly exceeds that of $He_{13}Kr^+$ if a drift field is applied;[4] $He_{12}Kr^+$ appears to be particularly stable. Lewerenz et al. measured mass spectra of helium droplets doped with krypton.[43] They reported an enhanced ion yield for $He_{10}Kr^+$, but the resolution was poor; krypton isotopes were not resolved. In similar experiments performed at higher resolution and involving single-photon ionization, Kim et al. reported enhanced ion yields for $He_{12}Kr^+$, $He_{12}Kr_2^+$, and $He_{12}Kr_3^+$.[7] In previous work, we have confirmed the anomaly for $He_{12}Kr^+$ but could not record reliable data for complexes containing more than one krypton atom.[8]

The present data (Figure 4) confirm the anomaly for $He_{12}Kr^+$, and they show another, weaker one for $He_{14}Kr^+$. The He_nKr^+ distribution is featureless for larger values of n, but a very broad maximum at around $n \approx 35$ appears in all of our data. Possible reasons for this feature, which is also observed for He_nXe^+ but not He_nAr^+, will be discussed in section 3C.

The difference in ionization energies between krypton (IE = 14.00 eV) and helium (24.59 eV) is even larger than that between argon (15.760 eV) and helium. Hence, one would expect negligible charge transfer between Kr^+ and He, and $He_{12}Kr^+$ might have an approximately icosahedral structure similar to that of $He_{12}Ar^+$ (we are not aware of any theoretical work pertaining to He_nKr^+, except for $HeKr^+$[64,65]). Concerning the anomaly at $He_{14}Kr^+$, it is worth noting that Murrell et al.[49] computed an abrupt drop in the dissociation energy of He_nAr^+ at $n = 14$ because two additional helium atoms could be squeezed into the first solvation shell ($He_{12}Ar^+$). The anomaly predicted for $n = 14$ was not observed in the He_nAr^+ data (Figure 3), but perhaps it shows up in He_nKr^+ thanks to the larger size of Kr^+; the less compact solvation shell in $He_{12}Kr^+$ would more easily accommodate two additional helium atoms.

The abundance of $He_nKr_2^+$ reveals two weak anomalies at $n = 7$ and 12 plus stronger ones at 18 and 20. Several very weak anomalies (at $n = 10$, 12, 16) are observed for $He_nKr_3^+$ plus stronger ones at $n = 24$ and 26. These results are inconsistent with work by Kim et al. who reported strong local maxima for $He_{12}Kr_2^+$ and $He_{12}Kr_3^+$.[7] In Figure 4b of Kim's work, the group of mass peaks assigned to $He_{12}Kr_2^+$ was about three times more intense than that for $He_{11}Kr_2^+$; in our work, the enhancement is less than 10%. We believe that the pronounced anomalies in Kim's work were caused by xenon impurities (the authors had doped helium droplets with either krypton or xenon). Xenon has nine naturally occurring isotopes. The most abundant one is ^{132}Xe (natural abundance 26.89%), while the most abundant isotope of krypton is ^{84}Kr. Thus, the nominal mass of ^{132}Xe equals that of the main isotopologue of $He_{12}Kr^+$; the exact masses differ by only 0.038 au.

In order to test our hypothesis that a $KrXe^+$ impurity was erroneously interpreted as a magic $He_{12}Kr_2^+$, and Kr_2Xe^+ as $He_{12}Kr_3^+$, we have simulated the corresponding mass spectra assuming a resolution better than 1 au but insufficient to separate nominally isobaric ions, in line with the experimental conditions in Kim's work.[7] A simulated spectrum of He_nKr_2 with equal ion abundance for all values of n is shown in Figure 2b (narrow bars); it has already been discussed in section 3A. Figure 2c shows a simulated spectrum of $He_nKr_2^+$ assuming a 50% higher abundance of $He_{12}Kr_2^+$; the extra contribution is shown explicitly by the wide bars. Figure 2d shows a simulated spectrum of $He_nKr_2^+$ with no magic $He_nKr_2^+$ but, instead, a 50% contamination with $KrXe^+$; the contribution is shown explicitly

dx.doi.org/10.1021/jp406540p | J. Phys. Chem. A 2014, 118, 8050−8059

by the wide bars. The two simulated spectra in Figure 2c and d are quite similar; both feature a local maximum at 216 au. The most telling difference between the two spectra is the enhancement at masses 213 and 215 au due to the abundant ^{129}Xe (26.44%) and ^{131}Xe (21.18%) isotopes. Such an enhancement is clearly visible in Figure 6 of Kim's paper.[7] We conclude that the very strong anomalies in the ion signal at around 216 and 300 au reported by Kim et al. were artifacts.

We note that $He_{12}Kr^+$ and Xe^+ are readily distinguished. Although their main isotopes (at nominal mass 132 au, with a mass difference of 0.039 au) would be barely resolvable, the He_nKr^+ series produces no peak at mass 129, whereas ^{129}Xe is nearly as abundant as ^{132}Xe. In our spectra, mass peaks at 129 au are below the 1% level of the peak at 132 au ($He_{12}{}^{84}Kr^+$), that is, a xenon impurity can be clearly ruled out.

Figure 4 reveals an interesting pattern. The pair of dominant anomalies in the abundance of $He_nKr_x^+$ shifts from (12,14) for $x = 1$ to (18,20) for $x = 2$ to (24,26) for $x = 3$, each time a shift by 6 units. Given the disparity in ionization energies between krypton and helium and the large dissociation energies of Kr_2^+ (about 1.3 eV[54,55]) and Kr_3^+ (0.25 eV[66]), the ionic core in $He_nKr_x^+$ will essentially be the Kr_x^+ ion, carrying close to 100% of the charge. An icosahedral arrangement of 12 He atoms in $He_{12}Kr^+$ may be viewed as consisting of two five-atom rings plus two He atoms at either end (plus, perhaps, another two atoms; see our discussion of $He_{14}Kr^+$). Upon solvation of Kr_2^+, a third ring containing six helium atoms would be inserted between the five-atom rings and another ring containing six helium atoms upon solvation of the linear Kr_3^+. Kr is significantly larger than He (the equilibrium distance of Kr_2 equals[67] 4.0 Å, while the distance between adjacent atoms in condensed helium is 2.97 Å[40]). Thus, it is reasonable to assume that the additional helium rings surrounding Kr_2^+ or Kr_3^+ would accommodate six rather than five atoms.

B.3. Xenon. Figure 5 reveals a weak anomaly in the abundance distribution of He_nXe^+ at $n = 12$ plus two broad maxima at around $n = 10$ and 35. The abundance distributions of $He_nXe_2^+$ and $He_nXe_3^+$ show only minor anomalies; the two broad maxima are absent. The broad features will be discussed in section 3C.

Helium−xenon complexes were investigated in three previous reports.[7,43,44] Toennies and co-workers reported three broad maxima at $n = 4$, 8, and 15 in the He_nXe^+ series, but the corresponding mass peaks were barely resolved.[43] Janda and co-workers[44] and Neumark and co-workers[7] reported mass spectra of He_nXe^+ and $He_nXe_2^+$ with unit mass resolution but without the ability to distinguish between different ions of the same nominal mass. They did not report any anomalies in the distribution of He_nXe^+. Xenon has nine naturally occurring isotopes, but only two have an odd atomic mass number, $A = 129$ and 131. Thus, below the mass of Xe_2^+, the ion series $He_n{}^{129}Xe^+$ and $He_n{}^{131}Xe^+$ are free from contributions from other helium−xenon isotopologues. The fact that no anomalies were noticed in previous work is probably due to a combination of low resolution and statistical fluctuations[44] or contaminants.[68]

Why is the anomaly at $He_{12}Xe^+$ so much weaker than that at $He_{12}Ar^+$ and $He_{12}Kr^+$? The $HeXe^+$ bond length is approximately 3.4 Å,[65,69] substantially larger than the He−He separation of 2.97 Å in condensed helium.[40] In a cluster, the bond length of $HeXe^+$ is probably >3.4 Å because of reduced charge delocalization. In a hypothetical icosahedral $He_{12}Xe^+$, such a large radial $HeXe^+$ distance would cause an even larger distance between adjacent peripheral helium atoms. In other words, helium atoms are too small to complete a solvation shell at $He_{12}Xe^+$.

The ion abundances of $He_nXe_2^+$ and $He_nXe_3^+$ cannot be reliably assessed unless one corrects for the various isotopologues. The most abundant isotope of xenon is ^{132}Xe (abundance 26.89%); six other isotopes occur with significant abundances, namely, ^{128}Xe (1.92%), ^{129}Xe (26.44%), ^{130}Xe (4.08%), ^{131}Xe (21.18%), ^{134}Xe (10.44%), and ^{136}Xe (8.87%). The problem of crosstalk discussed in section 3A is substantial. The matrix method provides a remedy, and as a result, we are able to identify weak anomalies in the abundance distributions of $He_nXe_2^+$ and $He_nXe_3^+$.

C. Broad Features in the Distributions of He_nKr^+ and He_nXe^+. The broad maxima at $n \approx 35$ in the abundance distributions of He_nKr^+ and He_nXe^+ (Figures 4 and 5) contrast with the distributions of complexes containing two or more heavy Ng atoms. The features, which could also be characterized as one broad minimum at around $n = 18$, appear in all our data for a variety of helium expansion conditions and partial pressures in the pick-up cell, that is, a variety of droplet sizes and Ng cluster sizes. Furthermore, they are absent from the abundance distribution of He_nAr^+. No specific structures can possibly account for such broad features. Instead, we tentatively draw a parallel to another striking difference between clusters of argon and clusters of heavy Ng's, namely, the experimentally established propensity of (bare) argon clusters to fragment upon ionization into mostly dimer ions, while clusters of heavy Ng's fragment overwhelmingly into monomer ions.[38,70] The difference is quite dramatic but not easily detected because in most experiments, the distribution of neutral clusters prior to ionization remains unknown; an elaborate setup involving elastic scattering between two supersonic beams is required to mass-select neutral clusters.[71]

In the experiments by Buck and co-workers,[38,70,71] bare Ng clusters were directly ionized by electrons, whereas in our experiments Ng clusters are embedded in helium droplets and ionized indirectly by charge transfer from He^+.[72−74] Still, experiments by Janda and co-workers suggest that these different experimental approaches both show the same striking difference in the fragmentation behavior between heavy Ng clusters and argon clusters.[5,44]

However, we cannot propose a specific mechanism that would account for the different abundance distributions between He_nNg^+ for heavy Ng's and He_nAr^+. Theoretical descriptions of the fragmentation dynamics of small clusters of argon, krypton, or xenon have struggled for a long time to explain the differences; dimer ions were invariably found to be the dominant fragment ions.[38,75] After all, the binding energies of Kr_2^+ and Xe_2^+ are nearly as strong as that of Ar_2^+.[54,55] Very recently, Janecek et al. have proposed a possible origin of the difference.[39] Their multiscale approach is complex; it involves spin−orbit coupling and different time scales to account for initial, nonadiabatic processes as well as radiative and nonradiative transitions between electronically excited states that occur on a microsecond time scale. Metastable dissociation of excited Ng dimer ions has been shown experimentally to occur on this time scale,[76−78] with profound differences between light (Ne, Ar) and heavy Ng's. It remains to be seen if excited states could possibly cause the peculiar broad features in the distributions of He_nKr^+ and He_nXe^+.

D. Relative Dissociation Energies of He_nNg^+. As discussed elsewhere, for clusters with small heat capacities

dx.doi.org/10.1021/jp406540p | J. Phys. Chem. A 2014, 118, 8050−8059

such as small He_nNg^+ ions, the evaporative model suggests that the relative abundance is proportional to the relative dissociation energy.[15,16] Here, the relative abundance is defined as the ratio of the observed abundance I_n and its local average $\langle I_n \rangle$, and the relative dissociation energy is defined as the ratio of D_n and its local average $\langle D_n \rangle$, hence

$$\frac{D_n}{\langle D_n \rangle} = \frac{I_n}{\langle I_n \rangle} \quad (2)$$

The relation has to be taken with some caution. First, its validity has not yet been tested. Second, there is no unique definition of the local averages. For extended data sets, a running average with Gaussian weighting is often used.[79] For small data sets, a fit with a polynomial is a better choice because points near the end of the data set (e.g., $n = 1$ or 2) would be lost otherwise.[16,80,81] In the present work, we have fitted fourth-degree polynomials. As an illustration, the dashed line in Figure 6a is a fourth-degree polynomial fit to the theoretical dissociation energies[49] of He_nAr^+ for $1 \leq n \leq 16$; the corresponding relative dissociation energies calculated from eq 2 are shown in Figure 6b. The measured relative abundances are shown in Figure 6c–e for Ar, Kr, and Xe, respectively. Also shown (Figure 6f) are data for He_nNe^+ that were recently recorded in our lab.[32] Contrary to previous, conceptually similar experiments[29−31] our data reveal a strong anomaly at $He_{13}Ne^+$, similar to the one observed by Kojima et al. in drift tube experiments.[4] However, calculated dissociation energies of He_nNe^+ either feature anomalies at $n = 10$ and 12[49] or none at all.[30,31]

The relative abundances in Figure 6 display more clearly local anomalies that tend to be masked if they occur in regions where I_n changes rapidly with n. Furthermore, they provide a better measure of the strength of an anomaly. $He_{12}Ar^+$ is enhanced by some 50%, $He_{13}Ne^+$ by some 40%, while the anomaly of $He_{12}Xe^+$ measures only 10%. We also see that the calculated[49] relative dissociation energies of He_nAr^+ (Figure 6b) do not track the relative abundance of these ions (Figure 6c); instead, they bear a resemblance to the relative abundance of He_nKr^+. Our main conclusions from Figure 6 are that (i) the computed dissociation energies of He_nAr^+ do not match the experimental results, (ii) the anomalies in the relative abundance decrease in strength from Ar to Kr to Xe, and (iii) anomalies in the abundance of He_nNe^+ differ markedly from those of Ar^+, Kr^+, and Xe^+ complexed with helium.

E. Bare Ng Clusters. The mass spectra also show the occurrence of bare Ng clusters Ng_x^+ or, in other words, $Ng_xHe_n^+$ complexes with $n = 0$ (see, e.g., the mass spectrum in Figure 1). We do not show their ion abundance in Figures 3–5, but some remarks are in order.

First, bare cluster ions Ng_x^+ ($x > 1$) result from ionization-induced fragmentation of helium droplets doped with Ng atoms because neutral Ng clusters can form only within a helium droplet, and Ng_x will not be expelled from the droplet until the droplet is ionized. The ion yield of Ng_x^+ relative to that of $Ng_xHe_n^+$ (where n is some small number >0) increases systematically as the mass of the Ng increases. For neon, the ion yield of Ne_x^+ with $x > 3$ is less than that of $Ne_xHe_n^+$ (for small n). For argon, bare cluster ions and mixed complexes have about the same yield, while for xenon, bare cluster ions are an order of magnitude more abundant. In short, fragmentation of doped helium droplets into bare Ng_x^+ appears to increase as the mass of the dopant increases.

Second, the trend described above for Ng_x^+ mirrors a trend observed by Janda and co-workers[44] and Neumark and co-workers[7] for Ng monomers; those authors have discussed possible reasons for this phenomenon. We cannot directly confirm their observations because in our experimental setup, there is a possibility that atomic Ng^+ results from leakage of the dopant gas from the pick-up cell to the ionizer rather than from ionization-induced fragmentation of doped helium droplets. We note, however, that Janda and co-workers[44] reported a similar trend for Ng dimer ions, and here, our data clearly agree with theirs.

4. CONCLUSIONS

We have reported mass spectra of helium droplets doped with argon, krypton, or xenon. The resolution of the mass spectrometer exceeds the resolution of instruments used in previous studies by an order of magnitude. This allows us to distinguish between ions of nominally identical mass. As a result, the abundance of the complete ion series $He_nNg_x^+$ can be established without interference from ions containing a different number of Ng atoms. Furthermore, a matrix method is used to account for isotopologues that cannot be resolved, such as $He_{10}{}^{86}Kr_2^+$, $He_{11}{}^{84}Kr_2^+$, $He_{12}{}^{82}Kr_2^+$, and $He_{12}{}^{80}Kr^{84}Kr^+$. A rich spectrum of anomalies is observed in the abundance distributions; several interesting patterns have been interpreted. Perhaps the most striking is evidence for the existence of three shells of helium atoms in a rigid icosahedral arrangement that solvate Ar^+. This conclusion runs counter to that of most theoretical studies of atomic cations in helium, which usually conclude that the effects of electrostriction are not strong enough to localize helium atoms outside of the first solvation shell. However, the theoretical treatment of charged complexes of Ng's with helium faces several challenges, including the nature of the ionic core, the extent of charge delocalization, and the effect of quantum effects including zero-point motion, its effect on the delocalization of the charge, and the bosonic nature of ^4He. The present experimental results provide a testing ground for future theoretical studies.

AUTHOR INFORMATION

Corresponding Authors

*E-mail: paul.scheier@uibk.ac.at. Tel: 0043 512 507 52660 (P.S.).

*E-mail: olof.echt@unh.edu. Tel: 001 603 862 3548 (O.E.).

Present Address

[#]C.L.: V&F Analyze and Messtechnik GmbH, 6067 Absam, Austria.

Notes

The authors declare no competing financial interest.

[§]E-mail: peterbartl@gmail.com (P.B.); christian.leidlmair@gmail.com (C.L.); stephan.denifl@uibk.ac.at (S.D.)

ACKNOWLEDGMENTS

P.B. acknowledges a dissertation grant from the vice-rectorate for research of the University of Innsbruck. This work was supported by the Austrian Science Fund, Wien (FWF Projects P19073, P23657, and L633).

REFERENCES

(1) Atkins, K. R. Ions in Liquid Helium. *Phys. Rev.* **1959**, *116*, 1339–1343.

(2) Glaberson, W. I.; Johnson, W. W. Impurity Ions in Liquid Helium. *J. Low Temp. Phys.* **1975**, *20*, 313−338.
(3) Hiraoka, K.; Shimizu, A.; Minamitsu, A.; Nasu, M.; Wasada, H.; Yamabe, S. Formation of the Trimer Ion Core in the Heterogeneous Rare Gas Cluster Ions. *J. Chem. Phys.* **1998**, *108*, 6689−6697.
(4) Kojima, T. M.; Kobayashi, N.; Kaneko, Y. Helium Cluster Ions $RgHe_x^+$ (Rg = Ne, Ar and Kr, $x \leq 14$) Formed in a Drift Tube Cooled by Liquid-Helium. *Z. Phys. D* **1992**, *22*, 645−650.
(5) Callicoatt, B. E.; Forde, K.; Ruchti, T.; Jung, L. L.; Janda, K. C.; Halberstadt, N. Capture and Ionization of Argon within Liquid Helium Droplets. *J. Chem. Phys.* **1998**, *108*, 9371−9382.
(6) Ferreira da Silva, F.; Bartl, P.; Denifl, S.; Echt, O.; Märk, T. D.; Scheier, P. Argon Clusters Embedded in Helium Nanodroplets. *Phys. Chem. Chem. Phys.* **2009**, *11*, 9791−9797.
(7) Kim, J. H.; Peterka, D. S.; Wang, C. C.; Neumark, D. M. Photoionization of Helium Nanodroplets Doped with Rare Gas Atoms. *J. Chem. Phys.* **2006**, *124*, 214301.
(8) Schöbel, H.; Bartl, P.; Leidlmair, C.; Denifl, S.; Echt, O.; Märk, T. D.; Scheier, P. High-Resolution Mass Spectrometric Study of Pure Helium Droplets, and Droplets Doped with Krypton. *Eur. Phys. J. D* **2011**, *63*, 209−214.
(9) Klots, C. E. Evaporation from Small Particles. *J. Phys. Chem.* **1988**, *92*, 5864−5868.
(10) Brechignac, C.; Cahuzac, P.; Leygnier, J.; Weiner, J. Dynamics of Unimlecular Dissocation of Sodium Cluster Ions. *J. Chem. Phys.* **1989**, *90*, 1492−1498.
(11) Klots, C. E. Kinetic Methods for Quantifying Magic. *Z. Phys. D* **1991**, *21*, 335−342.
(12) Casero, R.; Soler, J. M. Onset and Evolution of "Magic Numbers" in Mass Spectra of Molecular Clusters. *J. Chem. Phys.* **1991**, *95*, 2927−2935.
(13) Näher, U.; Hansen, K. Temperature of Large Clusters. *J. Chem. Phys.* **1994**, *101*, 5367−5371.
(14) Hansen, K.; Näher, U. Evaporation and Cluster Abundance Spectra. *Phys. Rev. A* **1999**, *60*, 1240−1250.
(15) Leidlmair, C.; Wang, Y.; Bartl, P.; Schöbel, H.; Denifl, S.; Probst, M.; Alcamí, M.; Martín, F.; Zettergren, H.; Hansen, K.; et al. Structures, Energetics and Dynamics of Helium Adsorbed on Isolated Fullerene Ions. *Phys. Rev. Lett.* **2012**, *108*, 076101.
(16) An der Lan, L.; Bartl, P.; Leidlmair, C.; Jochum, R.; Denifl, S.; Echt, O.; Scheier, P. Solvation of Na^+, K^+ and Their Dimers in Helium. *Chem.—Eur. J.* **2012**, *18*, 4411−4418.
(17) Müller, S.; Mudrich, M.; Stienkemeier, F. Alkali−Helium Snowball Complexes Formed on Helium Nanodroplets. *J. Chem. Phys.* **2009**, *131*, 044319.
(18) Theisen, M.; Lackner, F.; Ernst, W. E. Forming Rb^+ Snowballs in the Center of He Nanodroplets. *Phys. Chem. Chem. Phys.* **2010**, *12*, 14861−14863.
(19) Theisen, M.; Lackner, F.; Ernst, W. E. Cs Atoms on Helium Nanodroplets and the Immersion of Cs^+ into the Nanodroplet. *J. Chem. Phys.* **2011**, *135*, 074306.
(20) Döppner, T.; Diederich, T.; Gode, S.; Przystawik, A.; Tiggesbäumker, J.; Meiwes-Broer, K. H. Ion Induced Snowballs as a Diagnostic Tool to Investigate the Caging of Metal Clusters in Large Helium Droplets. *J. Chem. Phys.* **2007**, *126*, 244513.
(21) Ferreira da Silva, F.; Waldburger, P.; Jaksch, S.; Mauracher, A.; Denifl, S.; Echt, O.; Märk, T. D.; Scheier, P. On the Size of Ions Solvated in Helium Clusters. *Chem.—Eur. J.* **2009**, *15*, 7101−7108.
(22) Bartl, P.; Leidlmair, C.; Denifl, S.; Scheier, P.; Echt, O. Cationic Complexes of Hydrogen with Helium. *ChemPhysChem* **2012**, *14*, 227−232.
(23) Echt, O.; Kaiser, A.; Zöttl, S.; Mauracher, A.; Denifl, S.; Scheier, P. Adsorption of Polar and Non-Polar Molecules on Isolated Cationic C_{60}, C_{70}, and Their Aggregates. *ChemPlusChem* **2013**, *78*, 910−920.
(24) Slavicek, P.; Lewerenz, M. Snowballs, Quantum Solvation and Coordination: Lead Ions inside Small Helium Droplets. *Phys. Chem. Chem. Phys.* **2010**, *12*, 1152−1161.
(25) Galli, D. E.; Ceperley, D. M.; Reatto, L. Path Integral Monte Carlo Study of ^{4}He Clusters Doped with Alkali and Alkali-Earth Ions. *J. Phys. Chem. A* **2011**, *115*, 7300−7309.
(26) Calvo, F. Size-Induced Melting and Reentrant Freezing in Fullerene-Doped Helium Clusters. *Phys. Rev. B* **2012**, *85*, 060502(R).
(27) Shin, H.; Kwon, Y. Commensurate-Incommensurate Transition of ^{4}He Adsorbed on a Single C_{60} Molecule. *J. Chem. Phys.* **2012**, *136*, 064514.
(28) Marinetti, F.; Uranga-Pina, L. I.; Coccia, E.; Loopez-Duran, D.; Bodo, E.; Gianturco, F. A. Microsolvation of Cationic Dimers in ^{4}He Droplets: Geometries of $A_2^+(He)_N$ (A = Li, Na, K) from Optimized Energies. *J. Phys. Chem. A* **2007**, *111*, 12289−12294.
(29) Ruchti, T.; Förde, K.; Callicoatt, B. E.; Ludwigs, H.; Janda, K. C. Charge Transfer and Fragmentation of Liquid Helium Clusters That Contain One or More Neon Atoms. *J. Chem. Phys.* **1998**, *109*, 10679−10687.
(30) Seong, J.; Rohrbacher, A.; Li, Z. R.; Janda, K. C.; Tao, F. M.; Spiegelman, F.; Halberstadt, N. Potential Energy Surfaces for He_nNe^+ Ions: Ab Initio and Diatomics-in-Molecule Results. *J. Chem. Phys.* **2004**, *120*, 7456−7463.
(31) Brindle, C. A.; Prado, M. R.; Janda, K. C.; Halberstadt, N.; Lewerenz, M. Structure and Stability of Ne^+He_n: Experiment and Diffusion Quantum Monte Carlo Theory With "On the Fly" Electronic Structure. *J. Chem. Phys.* **2005**, *123*, 064312.
(32) Bartl, P.; Denifl, S.; Scheier, P.; Echt, O. On the Stability of Cationic Complexes of Neon with Helium — Solving an Experimental Discrepancy. *Phys. Chem. Chem. Phys.* **2013**, *15*, 16599−16604.
(33) Coccia, E.; Bodo, E.; Marinetti, F.; Gianturco, F. A.; Yildrim, E.; Yurtsever, M.; Yurtsever, E. Bosonic Helium Droplets with Cationic Impurities: Onset of Electrostriction and Snowball Effects from Quantum Calculations. *J. Chem. Phys.* **2007**, *126*, 124319.
(34) Coccia, E.; Bodo, E.; Gianturco, F. A. Nanoscopic Phase Changes in Doped ^{4}He Droplets. *Europhys. Lett.* **2008**, *82*, 23001.
(35) Buzzacchi, M.; Galli, D. E.; Reatto, L. Alkali Ions in Superfluid ^{4}He and Structure of the Snowball. *Phys. Rev. B* **2001**, *64*, 094512.
(36) Seong, J.; Janda, K. C.; Halberstadt, N.; Spiegelmann, F. Short-Time Charge Motion in He_n^+ Clusters. *J. Chem. Phys.* **1998**, *109*, 10873−10884.
(37) Calvo, F.; Naumkin, F. Y.; Wales, D. J. Interplay between Charge and Vibrational Delocalization in Cationic Helium Clusters. *J. Chem. Phys.* **2011**, *135*, 124308.
(38) Poterya, V.; Fárník, M.; Buck, U.; Bonhommeau, D.; Halberstadt, N. Fragmentation of Size-Selected Xe Clusters: Why Does the Monomer Ion Channel Dominate the Xe_n and Kr_n Ionization? *Int. J. Mass Spectrom.* **2009**, *280*, 78−84.
(39) Janecek, I.; Janca, T.; Naar, P.; Kalus, R.; Gadea, F. X. Multiscale Approach Combining Nonadiabatic Dynamics with Long-Time Radiative and Non-Radiative Decay: Dissociative Ionization of Heavy Rare-Gas Tetramers Revisited. *J. Chem. Phys.* **2013**, *138*, 044303.
(40) Toennies, J. P.; Vilesov, A. F. Superfluid Helium Droplets: A Uniquely Cold Nanomatrix for Molecules and Molecular Complexes. *Angew. Chem., Int. Ed.* **2004**, *43*, 2622−2648.
(41) An der Lan, L.; Bartl, P.; Leidlmair, C.; Schöbel, H.; Jochum, R.; Denifl, S.; Märk, T. D.; Ellis, A. M.; Scheier, P. The Submersion of Sodium Clusters in Helium Nanodroplets: Identification of the Surface → Interior Transition. *J. Chem. Phys.* **2011**, *135*, 044309.
(42) Bartl, P. *Rare Gas Cluster Ion Formation in Helium Nanodroplets*. Ph.D. Thesis, Universität Innsbruck, 2013.
(43) Lewerenz, M.; Schilling, B.; Toennies, J. P. Successive Capture and Coagulation of Atoms and Molecules to Small Clusters in Large Liquid Helium Clusters. *J. Chem. Phys.* **1995**, *102*, 8191−8206.
(44) Ruchti, T.; Callicoatt, B. E.; Janda, K. C. Charge Transfer and Fragmentation of Liquid Helium Droplets Doped with Xenon. *Phys. Chem. Chem. Phys.* **2000**, *2*, 4075−4080.
(45) Strictly speaking, all mass peaks that are marked in Figures 1 and 2a coincide with other isotopologues containing the same number of krypton but a different number of helium atoms. Their contributions

are below 4% for $He_n^{84}Kr^+$ and below 18% for $He_n^{84}Kr_2^+$. They are corrected for in the data analysis, as discussed at the end of section 3A.
(46) Leidlmair, C. *Electron Driven Reactions in Ultracold Fullerene Complexes*. Ph.D. Thesis, Universität Innsbruck, 2011.
(47) Kaiser, A.; Leidlmair, C.; Bartl, P.; Zöttl, S.; Denifl, S.; Mauracher, A.; Probst, M.; Scheier, P.; Echt, O. Adsorption of Hydrogen on Neutral and Charged Fullerene: Experiment and Theory. *J. Chem. Phys.* **2013**, *138*, 074311.
(48) The anomaly at $He_{12}Ar^+$ is also apparent in spectra reported in ref 43, although it coincides with a strong $He_2Ar_2^+$ signal.
(49) Murrell, J. N.; Naumkin, F. Y.; Griffiths, C. R. The Structures and Stabilities of Mixed Inert Gas Cluster Ions: $NeHe_n^+$ and $ArHe_n^+$. *Mol. Phys.* **2001**, *99*, 115−132.
(50) Sun, X. Y.; Li, Z. R.; Wu, D.; Sun, C. C.; Gudowski, S.; Tao, F. M.; Janda, K. C. Asymmetrical Linear Structures Including Three-Electron Hemibonds or Other Interactions in the (ABA)-Type Triatomic Cations: Ne_3^+, $(He−Ne−He)^+$, $(Ar−Ne−Ar)^+$, $(Ar−O−Ar)^+$, $(He−O−He)^+$, and $(Ar−He−Ar)^+$. *J. Chem. Phys.* **2005**, *123*, 134304.
(51) Hoare, M. R.; Pal, P. Statistics and Stability of Small Assemblies of Atoms. *J. Cryst. Growth* **1972**, *17*, 77−96.
(52) Kim, B.; Kwon, Y. Structural and Superfluid Properties of the ^{4}He Monolayer on a C_{28} Molecule. *J. Low Temp. Phys.* **2013**, *171*, 599−605.
(53) Svrcková, P.; Vítek, A.; Karlický, F.; Paidarová, I.; Kalus, R. Theoretical Modeling of Ionization Energies of Argon Clusters: Nuclear Delocalization Effects. *J. Chem. Phys.* **2011**, *134*, 224310.
(54) Hall, R.; Lu, Y.; Morioka, Y.; Matsui, T.; Tanaka, T.; Yoshii, H.; Hayaishi, T.; Ito, K. High-Resolution Threshold Photoelectron Spectroscopy of Rare-Gas Dimers. *J. Phys. B: At. Mol. Opt. Phys* **1995**, *28*, 2435−2451.
(55) Ha, T. K.; Rupper, P.; Wüest, A.; Merkt, F. The Lowest Electronic States of Ne_2^+, Ar_2^+ and Kr_2^+: Comparison of Theory and Experiment. *Mol. Phys.* **2003**, *101*, 827−838.
(56) Harris, I. A.; Kidwell, R. S.; Northby, J. A. Structure of Charged Argon Clusters Formed in a Free Jet Expansion. *Phys. Rev. Lett.* **1984**, *53*, 2390−2393.
(57) Miehle, W.; Kandler, O.; Leisner, T.; Echt, O. Mass Spectrometric Evidence for Icosahedral Structure in Large Rare Gas Clusters: Ar, Kr, Xe. *J. Chem. Phys.* **1989**, *91*, 5940−5952.
(58) Scheier, P.; Märk, T. D. Metastable Decay of Singly Charged Argon Cluster Ions Ar_n^+. *Int. J. Mass Spectrom. Ion Process.* **1990**, *102*, 19−44.
(59) Stace, A. J.; Moore, C. A Correlation between Structure and Reactivity in Ion Clusters. *Chem. Phys. Lett.* **1983**, *96*, 80−84.
(60) Lethbridge, P. G.; Delmistro, G.; Stace, A. J. Hard-Sphere Cluster−Ion Structures. *J. Chem. Phys.* **1990**, *93*, 1995−2001.
(61) Kuntz, P. J.; Valldorf, J. A DIM Model for Homogeneous Noble Gas Ionic Clusters. *Z. Phys.* **1988**, *8*, 195−208.
(62) Chen, Z. Y.; May, B. D.; Castleman, A. W. Ab Initio Potential-Energy Surface for Ar_3^+. *Z. Phys. D* **1993**, *25*, 239−246.
(63) von Issendorff, B.; Hofmann, A.; Haberland, H. Observation of Linear Isomers of the Ionized Rare Gas Tetramers Ar_4^+ and Xe_4^+. *J. Chem. Phys.* **1999**, *111*, 2513−2518.
(64) Grandinetti, F. Helium Chemistry: A Survey of the Role of the Ionic Species. *Int. J. Mass Spectrom.* **2004**, *237*, 243−267.
(65) Viehland, L. A.; Gray, B. R.; Wright, T. G. Interaction Potentials, Spectroscopy and Transport Properties of Rg^+−He (Rg = Ar−Rn). *Mol. Phys.* **2009**, *107*, 2127−2139.
(66) Kalus, R.; Paidarova, I.; Hrivnak, D.; Paska, P.; Gadea, F. X. Modelling of Kr_n^+ Clusters (n = 2−20). I. Structures and Energetics. *Chem. Phys.* **2003**, *294*, 141−153.
(67) Slavicek, P.; Kalus, R.; Paska, P.; Odvárková, I.; Hobza, P.; Malijevský, A. State-of-the-Art Correlated Ab Initio Potential Energy Curves for Heavy Rare Gas Dimers: Ar_2, Kr_2, and Xe_2. *J. Chem. Phys.* **2003**, *119*, 2102−2119.
(68) Significant deviations of the intensity ratio between $He_n^{129}Xe^+$ and $He_n^{131}Xe^+$ from the theoretical one (26.4/21.2) in Figure 4b of ref 7 reveal the presence of contaminants.
(69) Wright, T. G.; Breckenridge, W. H. Radii of Atomic Ions Determined from Diatomic Ion−He Bond Lengths. *J. Phys. Chem. A* **2010**, *114*, 3182−3189.
(70) Steinbach, C.; Farnik, M.; Buck, U.; Brindle, C. A.; Janda, K. C. Electron Impact Fragmentation of Size-Selected Krypton Clusters. *J. Phys. Chem. A* **2006**, *110*, 9108−9115.
(71) Buck, U.; Meyer, H. Electron Bombardment Fragmentation of Ar van der Waals Clusters by Scattering Analysis. *J. Chem. Phys.* **1986**, *84*, 4854−4861.
(72) Lewis, W. K.; Lindsay, C. M.; Bemish, R. J.; Miller, R. E. Probing Charge-Transfer Processes in Helium Nanodroplets by Optically Selected Mass Spectrometry (OSMS): Charge Steering by Long-Range Interactions. *J. Am. Chem. Soc.* **2005**, *127*, 7235−7242.
(73) Echt, O.; Märk, T. D.; Scheier, P. Molecules and Clusters Embedded in Helium Nanodroplets. In *Handbook of Nanophysics*; Sattler, K., Ed.; CRC Press: New York, 2010; Vol. *2* (Clusters and Fullerenes), Chapter 20.
(74) Shepperson, B.; Liu, J.; Ellis, A. M.; Yang, S. F. Communication: The Formation of Helium Cluster Cations Following the Ionization of Helium Nanodroplets: Influence of Droplet Size and Dopant. *J. Chem. Phys.* **2011**, *135*, 041101.
(75) Bonhommeau, D.; Bouissou, T.; Halberstadt, N.; Viel, A. Modelization of the Fragmentation Dynamics of Krypton Clusters (Kr_n, n = 2−11) Following Electron Impact Ionization. *J. Chem. Phys.* **2006**, *124*, 164308.
(76) Fedor, J.; Parajuli, R.; Matt-Leubner, S.; Echt, O.; Hagelberg, F.; Gluch, K.; Stamatovic, A.; Probst, M.; Scheier, P.; Märk, T. D. Probing Electronic States of Ne_2^+ and Ar_2^+ by Measuring Kinetic Energy Release Distributions. *Phys. Rev. Lett.* **2003**, *91*, 133401.
(77) Fedor, J.; Gluch, K.; Parajuli, R.; Matt-Leubner, S.; Echt, O.; Scheier, P.; Märk, T. D. Mechanisms and Dynamics of the Metastable Decay in Ar_2^+. *J. Chem. Phys.* **2004**, *121*, 7253−7258.
(78) Fedor, J.; Echt, O.; Gluch, K.; Matt-Leubner, S.; Scheier, P.; Märk, T. D. On the Role of the II(1/2g) State in Spontaneous Dissociation of Krypton and Xenon Dimer Ions. *Chem. Phys. Lett.* **2007**, *437*, 183−188.
(79) Prasalovich, S.; Hansen, K.; Kjellberg, M.; Popok, V. N.; Campbell, E. E. B. Surface Entropy of Rare-Gas Clusters. *J. Chem. Phys.* **2005**, *123*, 084317.
(80) Zöttl, S.; Kaiser, A.; Bartl, P.; Leidlmair, C.; Mauracher, A.; Probst, M.; Denifl, S.; Echt, O.; Scheier, P. Methane Adsorption on Graphitic Nanostructures: Every Molecule Counts. *J. Phys. Chem. Lett.* **2012**, *3*, 2598−2603.
(81) Kaiser, A.; Zöttl, S.; Bartl, P.; Leidlmair, C.; Mauracher, A.; Probst, M.; Denifl, S.; Echt, O.; Scheier, P. Methane Adsorption on Aggregates of Fullerenes: Site-Selective Storage Capacities and Adsorption Energies. *ChemSusChem* **2013**, *6*, 1235−1244.